JACS
JOURNAL OF THE AMERICAN CHEMICAL SOCIETY
Article
pubs.acs.org/JACS

New Redox States Observed in [FeFe] Hydrogenases Reveal Redox Coupling Within the H-Cluster

Agnieszka Adamska-Venkatesh,[†] Danuta Krawietz,[‡] Judith Siebel,[†] Katharina Weber,[†] Thomas Happe,[‡] Edward Reijerse,*[,†] and Wolfgang Lubitz*[,†]

[†]Max-Planck-Institut für Chemische Energiekonversion, Stiftstrasse 34-36, 45470 Mülheim an der Ruhr, Germany

[‡]Fakultät für Biologie und Biotechnologie, Lehrstuhl für Biochemie der Pflanzen, AG Photobiotechnologie, Ruhr Universität Bochum, Universitätsstraße 150, 44801 Bochum, Germany

Supporting Information

ABSTRACT: Active [FeFe] hydrogenases can be obtained by expressing the unmaturated enzyme in *Escherichia coli* followed by incubation with a synthetic precursor of the binuclear [2Fe] subcluster, namely: $[NEt_4]_2[Fe_2(adt)(CO)_4(CN)_2]$ (adt = $[S\text{-}CH_2\text{-}NH\text{-}CH_2\text{-}S]^{2-}$). The binuclear subsite $Fe_2(adt)(CO)_3(CN)_2$ is attached through a bridging cysteine side chain to a [4Fe-4S] subcluster already present in the unmaturated enzyme thus yielding the intact native "H-cluster". We present FTIR electrochemical studies of the [FeFe] hydrogenase from *Chlamydomonas reinhardtii*, CrHydA1, maturated with the precursor of the native cofactor $[Fe_2(adt)(CO)_4(CN)_2]^{2-}$ as well as a non-natural variant $[Fe_2(pdt)(CO)_4(CN)_2]^{2-}$ in which the bridging amine functionality is replaced by CH_2. The obtained active enzyme CrHydA1(adt) shows the same redox states in the respective potential range as observed for the native system ($E_{(ox/red)}$ = −400 mV, $E_{(red/sred)}$ = −470 mV). For the $H_{ox} \rightarrow H_{red}$ transition the reducing equivalent is stored on the binuclear part, ($[4Fe\text{-}4S]^{2+}Fe^{II}Fe^{I} \rightarrow [4Fe\text{-}4S]^{2+}Fe^{I}Fe^{I}$), while the $H_{red} \rightarrow H_{sred}$ transition is characterized by a reduction of the [4Fe-4S] part of the H-cluster ($[4Fe\text{-}4S]^{2+}Fe^{I}Fe^{I} \rightarrow [4Fe\text{-}4S]^{+}Fe^{I}Fe^{I}$). A similar transition is reported here for the CO inhibited state of the H-cluster: ($[4Fe\text{-}4S]^{2+}Fe^{I}Fe^{II}CO \rightarrow [4Fe\text{-}4S]^{+}Fe^{I}Fe^{II}CO$). An FTIR electrochemical study of the inactive variant with the pdt ligand, CrHydA1(pdt), identified two redox states H^{pdt}-ox and H^{pdt}-"red". Both EPR and FTIR spectra of H^{pdt}-ox are virtually identical to those of the H^{adt}-ox and the native H_{ox} state. The H^{pdt}-"red" state is also characterized by a reduced [4Fe-4S] subcluster. In contrast to CrHydA1(adt), the H^{pdt}-ox state of CrHydA1(pdt) is stable up to rather high potentials (+200 mV). This study demonstrates the distinct redox coupling between the two parts of the H-cluster and confirms that the $[4Fe\text{-}4S]_H$ subsite is also redox active and as such an integral part of the H-cluster taking part in the catalytic cycle.

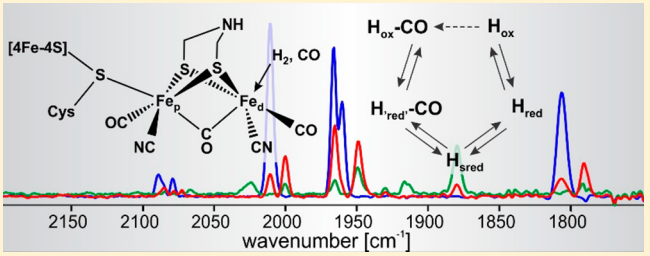

1. INTRODUCTION

Hydrogenases are metalloenzymes which catalyze both the production and oxidation of H_2 and are therefore of high interest for a future biohydrogen technology.[1−11] Since [FeFe] hydrogenases are the most active enzymes in hydrogen production *in vivo*, a detailed understanding of their catalytic mechanism is of great interest for developing artificial hydrogen production systems.[12,13] The active site of this enzyme is highly conserved and is referred to as the "H-cluster".[7,14−17] It contains a "classical" $[4Fe\text{-}4S]_H$ cluster coupled via one of its coordinating cysteine side groups to a unique binuclear subcluster $[2Fe]_H$, which is coordinated by CN^- and CO ligands as well as a dithiolate bridging ligand.[16−23] Recent studies showed that various biomimetic complexes modeling the binuclear subcluster can be inserted directly or with the help of the maturation factor HydF into unmaturated [FeFe] hydrogenases that only contain the $[4Fe\text{-}4S]_H$ part of the H-cluster.[24,25] However, only the insertion of the binuclear cofactor containing the amine group in the dithiolate bridging ligand (adt) leads to the assembly of the native H-cluster (see Figure 1) and affords fully active enzyme.[24,25]

During the catalytic process of hydrogen conversion the iron centers in the H-cluster change their oxidation states.[7] In the most oxidized active redox state called H_{ox} the binuclear subcluster is in the mixed valence $Fe^{I}Fe^{II}$ state while the [4Fe-4S] cluster is oxidized (2+).[7,26,27] This state is paramagnetic and shows a characteristic EPR signal with g = [2.10, 2.037, 1.996].[27] Upon a fully reversible one-electron reduction (−400 mV for the native [FeFe] hydrogenase from *Chlamydomonas reinhardtii*: CrHydA1) H_{ox} is converted into the active reduced state H_{red} which has the binuclear site presumably in an $Fe^{I}Fe^{I}$ (S = 0) configuration.[7,28] A subsequent fully reversible one-electron reduction (−460 mV for native CrHydA1) causes conversion of H_{red} to the "super reduced" active state H_{sred}.[28] EPR studies showed that H_{sred} is paramagnetic and gives a signal characteristic for a reduced $[4Fe\text{-}4S]^+$ cluster.[26] According to our previously

Received: April 4, 2014
Published: July 15, 2014

   dx.doi.org/10.1021/ja503390c | J. Am. Chem. Soc. 2014, 136, 11339−11346

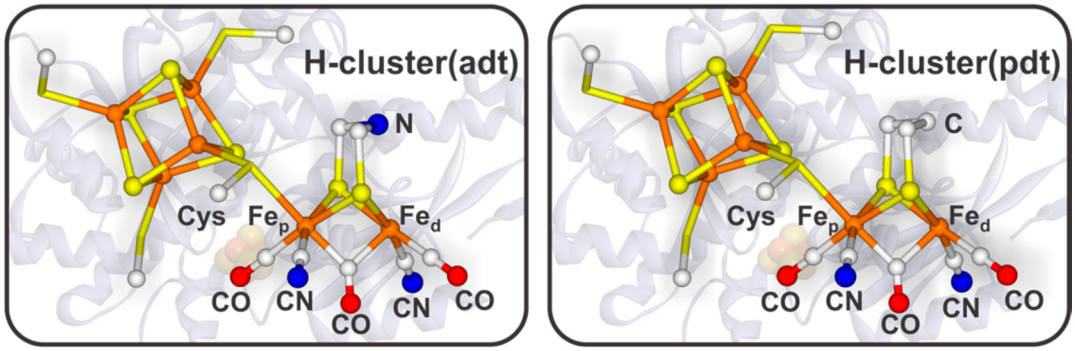

Figure 1. Structure of the active site (H-cluster) of artificially maturated [FeFe] hydrogenase with natural (H^{adt}) and non-natural (H^{pdt}) binuclear subsite.

proposed mechanism all these states are involved in the catalytic cycle.[26] In protein film electrochemistry (PFE) it was observed that CrHydA1 is very active over a large potential range and especially at low potentials shows high turnover rates in hydrogen production.[29]

The H-cluster of the active protein can be inhibited by CO generating the H_{ox}-CO state.[7,15,30] The electronic structure of H_{ox}-CO is similar to that of H_{ox} and is characterized by a mixed valence ($Fe^{I}Fe^{II}$) subsite in combination with an oxidized $[4Fe\text{-}4S]_H^{2+}$ subcluster.[7] The characteristic EPR and FTIR spectra of H_{ox}-CO are often observed in [FeFe] hydrogenase preparations that are exposed to light and/or oxygen. In this case the CO inhibited state is generated by the so-called "cannibalization process" in which the CO ligands released from destroyed H-clusters are captured by H-clusters that are still intact.[31,32] Up to now, no redox activity of the H_{ox}-CO state has been reported. In fact, a recent protein film electrochemical study in combination with DFT calculations indicated that reduction of H_{ox}-CO leads to damage or even dissociation of the H-cluster.[33]

In the current study we present FTIR spectroelectrochemical investigations of artificially maturated CrHydA1 using both the precursor of the native [2Fe] cofactor $[Fe_2(adt)(CO)_4(CN)_2]^{2-}$ and the non-natural variant $[Fe_2(pdt)(CO)_4(CN)_2]^{2-}$ in which the central bridging amine (NH) function is substituted by CH_2 (see Figure 1). For the native "hybrid protein" CrHydA1(adt) also the CO-inhibited state was investigated. We show that both CrHydA1(adt) under CO and CrHydA1(pdt) exhibit a redox transition which most likely involves the $[4Fe\text{-}4S]_H$ subsite.

2. EXPERIMENTAL SECTION

The synthesis of the $[Fe_2(adt)(CO)_4(CN)_2]^{2-}$ and $[Fe_2(pdt)(CO)_4(CN)_2]^{2-}$ biomimetic complexes followed previously published protocols.[34−36] Crystalline compounds were dissolved in DMSO and then diluted in Tris/HCl pH 8.0 buffer or directly dissolved in the buffer and handled strictly anaerobically.

$CrHydA1^{\Delta EFG}$ (hydrogenase expressed without maturases) was produced in *Escherichia coli* as described earlier.[25,37] The *in vitro* maturation of the [FeFe] hydrogenase was also described previously.[25] All steps were carried out under strict anaerobic conditions. CrHydA1 was prepared in 100 mM Tris/HCl pH 8.0, 2 mM sodium dithionate buffer with addition of 100 mM KCl to samples on which electrochemical experiments were performed. Oxidized samples were prepared by FTIR monitored stepwise titration with thionine.

Fourier transform infrared (FTIR) measurements were carried out using a Bruker IFS 66v/s FTIR spectrometer equipped with a nitrogen cooled Bruker mercury cadmium telluride (MCT) detector. The spectra were accumulated in the double-sided, forward−backward mode with 1000 scans (14 min) and a resolution of 2 cm^{-1} at 15 °C. Data processing was facilitated by home written routines in the MATLAB programming environment.

All spectroelectrochemical experiments were performed using a home-built electrochemical IR cell, constructed according to an original design by Moss et al.[7,38] Samples were loaded in between two CaF_2 windows on an electrochemically reduced gold mesh (approximately 50 μm thick) in electrical contact with the platinum counter electrode. An Ag/AgCl (1 M KCl) electrode was used as reference and was calibrated before and after each measurement by reduction/oxidation of methyl viologen. All potentials are listed versus the normal hydrogen electrode (NHE), and the uncertainty of the midpoint potentials was estimated to be ±20 mV. In the titrations the potential was controlled by an Autolab PGSTAT101 potentiostat using the Nova software. Since no mediators were used an extended equilibration time period of 30 min was applied at each potential. The temperature was controlled by a Huber Minichiller, and all experiments were performed at 15 °C.

Q-band EPR spectra were recorded using free induction decay (FID) detected EPR with a microwave pulse length of 1 μs. All pulse experiments were performed on a Bruker ELEXYS E580 Q-band spectrometer with a SuperQ-FT microwave bridge and a home-built resonator described earlier.[39] The magnetic field was calibrated using a Bruker ER035D NMR gaussmeter. X-band continuous wave (CW) EPR measurements were performed on a Bruker ELEXYS E-580 X-band spectrometer with a SuperX-FT microwave bridge and Bruker ER EN4118X-MD5 dielectric resonator. Cryogenic temperatures (10−20 K) were obtained by an Oxford CF935 flow cryostat. For the interpretation of all EPR experimental data, a home written simulation program (based on the EasySpin package)[40] in MATLAB was used.

3. RESULTS AND DISCUSSION

3.1. FTIR Electrochemistry for CrHydA1(adt) (Active Hybrid Enzyme). Figure 2A shows selected FTIR spectra of CrHydA1(adt) recorded during electrochemical oxidation. The potentials were chosen such that in each spectrum one of the well-known redox states H_{ox}, H_{red}, and H_{sred} has its maximum contribution.[28] In Figure 2B the intensities of one representative CO band for each of the states H_{ox}, H_{red}, and H_{sred} is plotted against the redox potential in the FTIR cell. Two fully reversible one-electron transitions with midpoint potentials in agreement (within experimental uncertainty) with the previously reported values for the native CrHydA1 hydrogenase were observed.[28] No signal loss occurred upon reduction from H_{red} to H_{sred} and reoxidation back to H_{red} (see Supporting Information). This suggests that no irreversible damage takes place at low potentials. A different situation is observed at high potentials. Above −300 mV the intensity of the oxidized state rapidly decreases (see Figure 2B), which can be attributed to irreversible damage of the H-cluster and release of the CO ligands. At the same time, an increase of the signal originating from the CO inhibited state (H_{ox}-CO) is observed corresponding to the "cannibalization

dx.doi.org/10.1021/ja503390c | J. Am. Chem. Soc. 2014, 136, 11339−11346

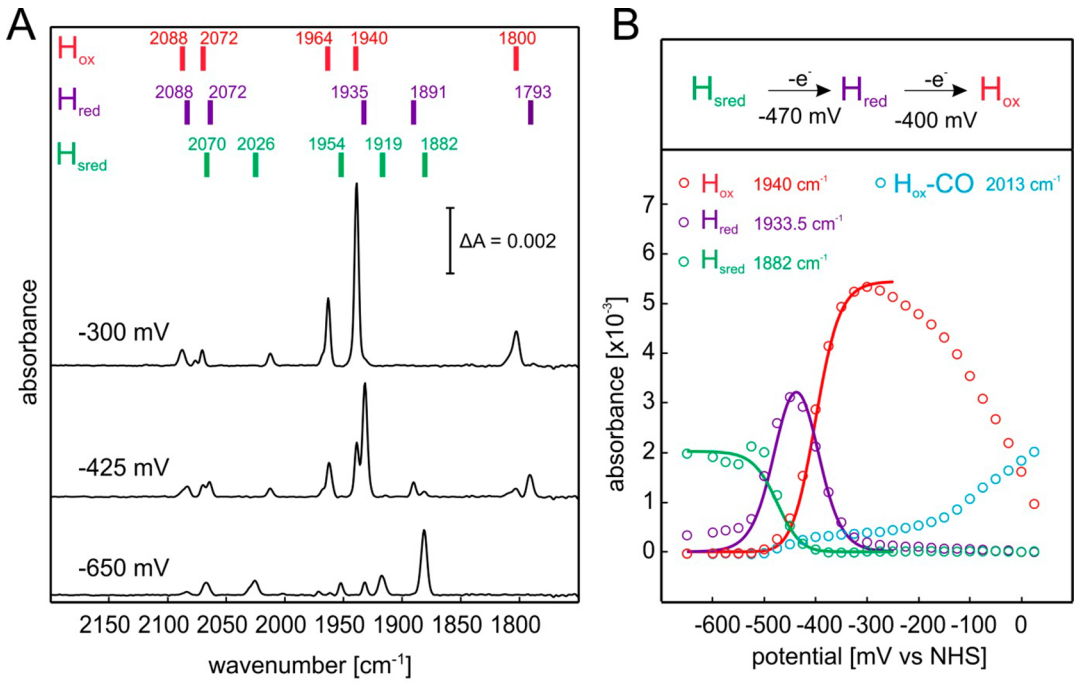

Figure 2. (A) Selected IR spectra of 1 mM CrHydA1(adt) in 100 mM Tris/HCl buffer pH 8.0, 100 mM KCl, 2 mM sodium dithionate at different redox potentials measured at 15 °C. At the top of the figure the band positions of the active states are indicated.[28] In the spectra taken at −300 and −425 mV also a fraction of H_{ox}-CO (signal position: 2092, 2084, 2013, 1970, 1964, and 1810 cm^{-1}) is present. (B) Oxidative titration of the active enzyme. The red circles correspond to the intensity of the most prominent CO band of the H_{ox} state at 1940 cm^{-1}, violet circles represent the signal at 1933.5 cm^{-1} characteristic for H_{red}, green circles indicate the signal at 1882 cm^{-1} of H_{sred}, while the light-blue circles indicate the band amplitude at 2013 cm^{-1} of the H_{ox}-CO state. The solid lines correspond to n = 1 Nerstian curves, $E_{ox/red}$ = −400 mV ± 20 mV and $E_{red/sred}$ = −470 mV ± 20 mV.

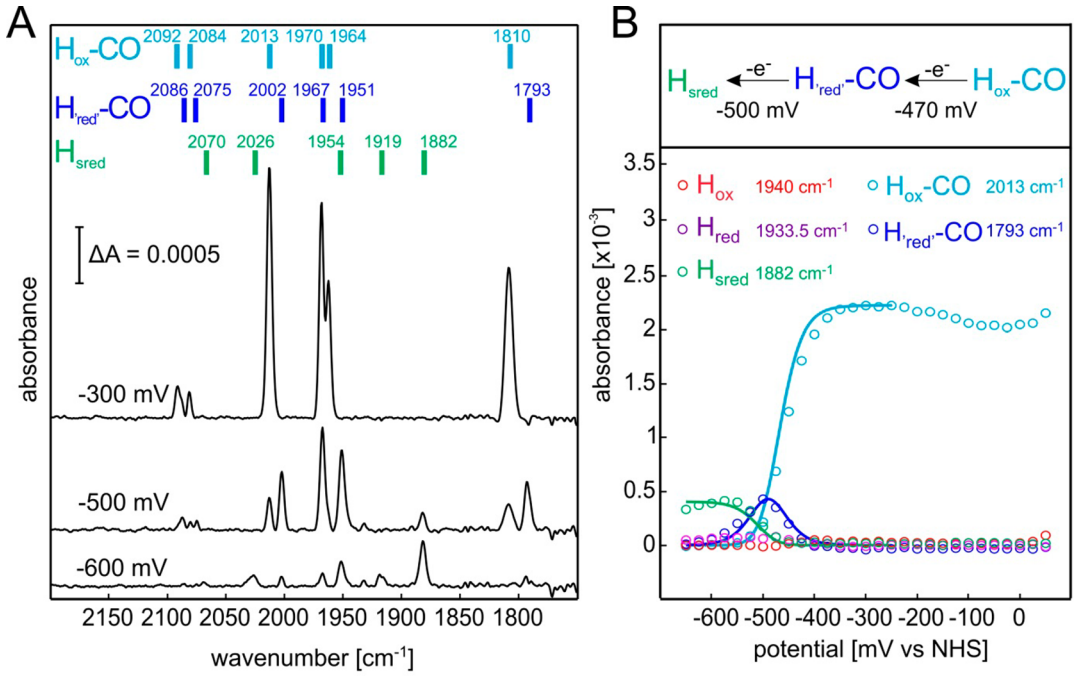

Figure 3. (A) Selected IR spectra of CrHydA1(adt) under CO gas at different redox potentials measured at 15 °C. The top of the figure shows the signal positions of the observed redox states.[28] (B) Reductive titration of the CO inhibited enzyme. The red circles correspond to intensity of the most prominent CO band of the H_{ox} state at 1940 cm^{-1}, violet circles to the signal at 1933.5 cm^{-1} characteristic for H_{red}, the green ones to 1882 cm^{-1} of H_{sred}, the light blue ones to 2013 cm^{-1} from the H_{ox}-CO state, and the blue ones to 1793 cm^{-1} of the $H_{red'}$-CO state. The solid lines correspond to n = 1 Nerstian curves, $E_{ox\text{-}CO/'red'\text{-}CO}$= −470 mV ± 20 mV and $E_{'red'\text{-}CO/sred}$ = −500 mV ± 20 mV.

effect".[31,32] It is interesting to note that in this type of experiment no reversible transition to a "super oxidized" state is observed.[32] This is in contrast to the situation in PFE experiments where for many [FeFe] hydrogenases the cyclic voltammogram shows a reversible oxidative inhibition at high potentials.[12,41] However, this discrepancy could be related to the different experimental

dx.doi.org/10.1021/ja503390c | J. Am. Chem. Soc. 2014, 136, 11339−11346

conditions in the respective electrochemical cells. For example, a recent study by Leger et al. showed that reversible oxidative inactivation at high potentials is facilitated by the presence of H_2 which, apparently, stabilizes high potential inactive states of the H-cluster.[42]

3.2. FTIR Electrochemistry on CrHydA1(adt) in the Presence of CO (Reductive Titration). By keeping the sample at high potential (+50 mV) the H-clusters are progressively disintegrated leading to a decreasing intensity of the H_{ox} signal and a steady increase of the H_{ox}-CO signal until eventually only this species remains in FTIR. It is estimated that this harsh procedure leaves approximately 20−25% (see Supporting Information) of the H-clusters as H_{ox}-CO, while the rest is disintegrated and the released CO and CN ligands are no longer iron bound and therefore do not show up in the FTIR range of the H-cluster. The sample can now be considered as CO inhibited [FeFe] hydrogenase. Upon reducing the redox potential from 50 to −300 mV the signal intensity from H_{ox}-CO does not change suggesting that no further damage occurs (see Figure 3B).

Lowering the potential further results in a decrease of the signal from H_{ox}-CO and the appearance of new signals at 2086 and 2075 cm^{-1} assigned to the CN^- ligands as well as signals at 2002, 1967, and 1951 cm^{-1} which are assigned to coupled vibrations of terminal CO ligands and finally a signal at 1793 cm^{-1} which is typical for a bridging CO ligand. The maximum of this new signal is reached at −500 mV (see Figure 3A). The FTIR peak positions of this signal were previously observed in FTIR spectra obtained for heterologously expressed CrHydA1 flushed with CO gas.[25,37] However, at that time these signals could not be assigned to a particular H-cluster state. From the current experiment we must conclude that this new signal is associated with a one-electron reduced CO inhibited state. The small shifts of the CO bands (in the range 3−17 cm^{-1}) with respect to the H_{ox}-CO spectrum as well as the midpoint potential of −470 mV, which is the same as $E_{red/sred}$, would suggest that reduction takes place on the $[4Fe\text{-}4S]_H$ cluster generating a $[4Fe\text{-}4S]^+$ configuration. To further support this hypotheses experiments involving light induced ^{13}CO scrambling were carried out and presented in Supporting Information (Figure S9).[32] Figure 4 presents the shift of the IR bands originating from the CO ligands of CrHydA1(adt) in the CO inhibited states after stepwise replacement of ^{12}CO by ^{13}CO: (i) exposure to ^{13}CO in the dark; and (ii) CO scrambling by illumination. It was confirmed that the 2002 cm^{-1} band from $H_{red'}$-CO corresponds to the band at 2013 cm^{-1} from H_{ox}-CO and the 1967 cm^{-1} band corresponds to that at 1970 cm^{-1}. These two bands were previously assigned to ν_{sym} and ν_{asym} of the two vibrationally coupled terminally CO ligands bound to the distal iron.[32] Thus, the largest shift is observed for the band assigned to the CO ligand bound to the proximal iron from 1964 cm^{-1} (H_{ox}-CO) to 1951 cm^{-1} ($H_{red'}$-CO). Although FTIR does not provide *direct* information on the oxidation state of the H-cluster, given the very small difference in the band positions of both states a change of the oxidation state of Fe_d seems very unlikely. The maximum intensity of the so-called $H_{red'}$-CO signal is observed around −500 mV. Already at this potential the signal originating from the H_{sred} state appears. Further lowering of the potential leads to complete conversion into the super reduced state (H_{sred}) (with CO release) leaving the binuclear center in the Fe^IFe^I form. No signals characteristic for oxidized (H_{ox}) and reduced states (H_{red}) were observed during this titration.

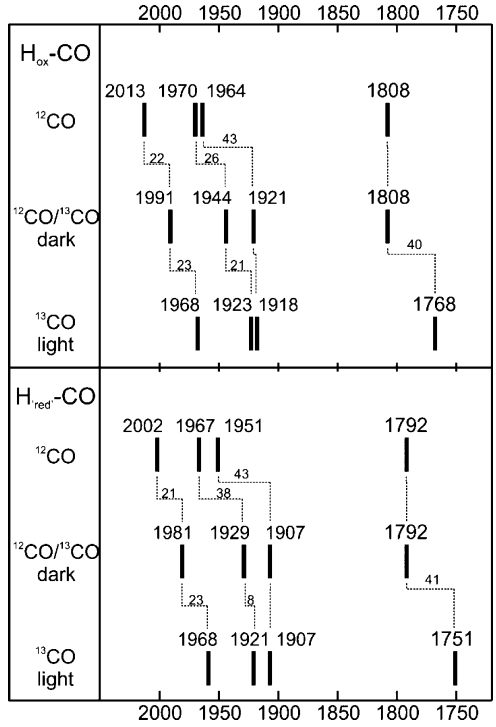

Figure 4. Overview of shifts of IR bands originating from the CO ligands of CrHydA1(adt) in the CO inhibited states upon replacing ^{12}CO by ^{13}CO. The first rows in both panels display the band positions for the samples prepared under ^{12}CO. The middle rows show the shifted band positions resulting from ^{13}CO treatment in the dark. For these samples only one distal CO and (surprisingly) the proximal CO is exchanged to ^{13}CO. In the last rows the band positions upon complete ^{13}CO exchange (scrambling by illumination) are presented.

The CO inhibition of various [FeFe] hydrogenases was studied extensively by PFE experiments as well as through DFT calculations.[33,41,43] It was observed that at high potentials CO inhibition is complete and fully reversible, while at low potentials it is not. From these observations it was concluded that CO strongly binds to the H_{ox} state and less tightly to H_{red} leading to partial but irreversible damage of the H-cluster.[33,41] It should be noted, however, that the individual redox states cannot be observed in these experiments since the protein is under turnover. Therefore, all redox states involved in the active cycle will occur. DFT studies predict that binding of CO to the H_{red} state, where the H-cluster is in the $[4Fe\text{-}4S]^{2+}$ Fe^IFe^I configuration, causes elongation of the Fe-S_{cys} distance and subsequent cleavage of this bond.[33] However, our experiments show that the oxidized CO inhibited state is present in a potential range where both uninhibited oxidized and reduced states can also occur. Also no signal originating from a released binuclear site was observed (see original spectra in Supporting Information) suggesting no dissociation of the binuclear site. DFT calculations also show that H_{sred} has a very low affinity for CO and that the structural integrity of the H-cluster would be maintained in this state.[33] This would explain why after the second reduction the extrinsic CO ligand is released and the super reduced state is formed. The reduced CO inhibited configuration observed in our experiments $[4Fe\text{-}4S]^+Fe^IFe^{II}$ was however not considered in these DFT studies and turns out to be perfectly stable.

Protein film electrochemistry studies by Armstrong and co-workers of three [FeFe] hydrogenases, including CrHydA1,

dx.doi.org/10.1021/ja503390c | J. Am. Chem. Soc. 2014, 136, 11339−11346

under addition of CO have revealed that the relative inhibition of the enzyme as a function of the applied electrochemical potential can be divided into three ranges, each separated by a one-electron redox transition.[43] In the high potential range, where H_{ox} should be present, the active site is strongly inhibited by CO (90%) while in the lowest potential range, where H_{sred} should be accumulated, activity is hardly affected (10%).[43] The middle range (presumably H_{red}) shows around 75% inhibition. These data would suggest that under turnover conditions at the electrode H_{red} can be inhibited to a certain extent, thus implicating a CO binding event. Our data are in agreement with these observations and allow us to postulate that also in other [FeFe] hydrogenases a "reduced" CO inhibited state may exist. However, in these multidomain [FeFe] hydrogenases, $H_{red'}$-CO similar to H_{sred}, does not occur as a resting state because the reduced $[4Fe\text{-}4S]_H$ subcluster is quickly reoxidized through the redox coupling with the accessory [4Fe-4S] clusters.[7,26]

3.3. FTIR Electrochemistry for CrHydA1(adt) in the H_{sred} State in the Presence of CO. In Figure 5 the oxidative titration of the H_{sred} sample under CO obtained at the end of the previous run (section 3.2) is presented. Figures 3B and 5 show that also under CO, the intensity of the signal originating from the super

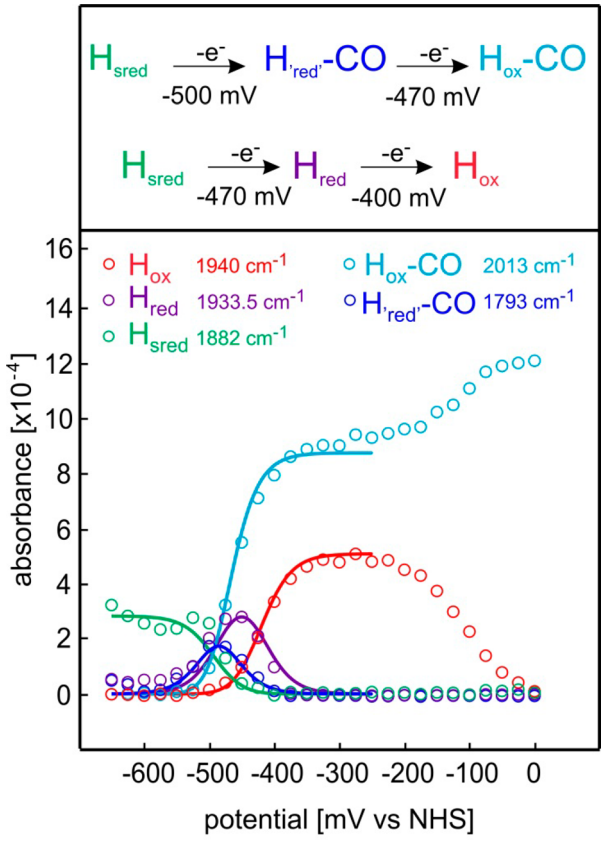

Figure 5. Oxidative titration of CrHydA1(adt) in the presence of CO gas. The red circles correspond to the intensity of the most prominent CO band of the H_{ox} state at 1940 cm^{-1}, violet circles to the signal at 1933.5 cm^{-1} characteristic for H_{red}, the green ones belong to 1882 cm^{-1} from H_{sred}, the light blue ones to 2013 cm^{-1} from the H_{ox}-CO state and the blue ones to 1793 cm^{-1} from the $H_{red'}$-CO state. The solid lines correspond to n = 1 Nerstian curves, $E_{ox/red}$ = −400 mV ± 20 mV, $E_{red/sred}$ = −470 mV ± 20 mV, $E_{ox\text{-}CO/'red'\text{-}CO}$ = −470 mV ± 20 mV and $E_{'red'\text{-}CO/sred}$ = −500 mV ± 20 mV.

reduced state does not change which indicates that no H-cluster destruction occurs. Figure 5 shows that during H_{sred} oxidation in the presence of CO, two processes take place: The reduced CO inhibited state ($H_{red'}$-CO) reappears and further converts into the H_{ox}-CO state. Simultaneously, as was previously observed during the titration without CO, conversion from H_{sred} to H_{red} and subsequently to H_{ox} occurs. This indicates that reactivation of the CO inhibited sample proceeds through the H_{sred} state. The fact that upon oxidation of H_{sred} not all H-clusters are converted back into the $H_{red'}$-CO state may be related to CO gas diffusing out of the electrochemically active volume of the FTIR cell thereby reducing effective CO partial pressure in the cell.

The observations described above allow us to construct the scheme shown in Figure 6 presenting two fully reversible

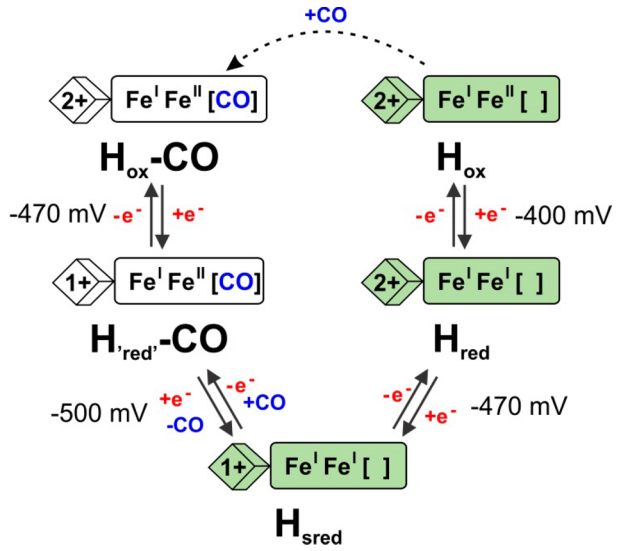

Figure 6. Schematic representation of the redox state conversion with and without CO gas. Under CO the oxidation of H_{sred} to H_{ox}-CO proceeds through $H_{red'}$-CO as an intermediate state, while without CO the "active" oxidation path is chosen along the catalytic states H_{red} and H_{ox}. Redox states involved in the catalytic cycle are marked in green.[26] The scheme representing the catalytically active cycle is presented in the Supporting Information.

"pathways": one CO inhibited path and a second active path, joined through the super reduced state. It is shown that artificially maturated [FeFe] hydrogenase behaves exactly the same way as the native enzyme; when no external CO is present the active oxidative path is chosen. With increasing CO partial pressure, the CO-path will become more dominant. It is interesting that even though the active sites of [FeFe] and [NiFe] hydrogenases are structurally very different they show a parallel behavior of their redox processes in the presence of extrinsic CO. Also in [NiFe] hydrogenase the most reduced state cannot be inhibited by CO gas and during its oxidation two CO inhibited states separated by one-electron transition are appearing.[7,44]

3.4. FTIR Electrochemistry and EPR Studies on CrHydA1(pdt). In recent studies it was demonstrated that the non-natural cofactor $[Fe_2(pdt)(CO)_4(CN)_2]^{2-}$, in which the bridging amine group is changed from NH to CH_2, can be incorporated into the unmaturated [FeFe] hydrogenase (containing only the [4Fe-4S] cluster).[24,25] It was also shown that this hybrid does not have any significant hydrogenase activity. At the same time it was noted that its FTIR spectrum (with band positions 2084 and 2065 cm^{-1} for the CN^- ligands,

dx.doi.org/10.1021/ja503390c | J. Am. Chem. Soc. 2014, 136, 11339−11346

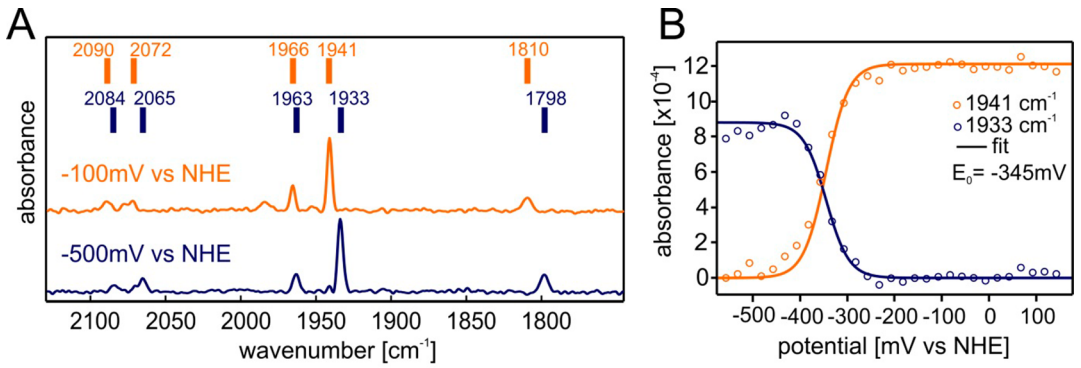

Figure 7. (A) Selected IR spectra of CrHydA1(pdt) at different redox potentials measured at 15 °C. On top the signal positions of the observed redox states are indicated. (B) Oxidative titration of the enzyme. The orange circles correspond to the intensity of the most prominent CO band of the oxidized state at 1941 cm^{-1} and the dark-blue circles to the signal at 1933 cm^{-1} characteristic for the reduced form. The solid lines correspond to $n = 1$ Nerstian curves, $E_{oxidized/reduced} = -345$ mV ± 20 mV.

1963 and 1933 cm^{-1} for the terminal CO ligands and 1798 cm^{-1} for the bridging CO ligand) strongly resembles that of the H_{ox} state of the native hydrogenase (see Figure 7A).

Figure 7B shows the FTIR monitored electrochemical titration of the CrHydA1(pdt) hybrid. Although inactive, the enzyme still shows one fully reversible one-electron redox transition. The originally reported signal[24,25] belongs to the reduced form, whereas the oxidized state is characterized by a very similar signal with slightly shifted band positions at 2090 and 2072 cm^{-1} for the CN^- ligands, 1966 and 1941 cm^{-1} for the terminal CO ligands and 1810 cm^{-1} for the bridging CO as depicted in Figure 7A. In both oxidation states the bridging CO is present as well as two bands from terminal CO ligands indicating that the additional CO ligand from the biomimetic complex was released upon insertion and that the open coordination site at the distal iron still should be present. Short exposure of the sample to low amounts of oxygen leads to complete loss of the H-cluster FTIR signature. However, despite the high oxygen sensitivity of this CrHydA1(pdt) hybrid no CO inhibited form could be identified. The nonaccessibility of the open coordination site might be related to the distortion of the bridging headgroup which is not able to create hydrogen bonds with the surrounding protein environment thereby blocking access for CO. The phenomenon will be investigated in more detail in a future study.

It is demonstrated in Figure 7B that in contrast to CrHydA1(adt) destruction of the active site occurs neither at low (−550 mV) nor at high potentials (+150 mV). This would suggest that turnover of the native enzyme and the active CrHydA1(adt) hybrid at high potentials leads to damage of the H-cluster. Presumably, the redox transition to the overoxidized state ($[4Fe\text{-}4S]^{2+}Fe^{II}Fe^{II}$) which is unstable in CrHydA1, occurs at much higher potential for CrHydA1(pdt).

The EPR spectrum recorded for the oxidized form of CrHydA1(pdt) shown in Figure 8 resembles the H_{ox} state of the native system with g values [2.094, 2.039, 1.998] which suggests that this form can be described by an oxidized $[4Fe\text{-}4S]^{2+}$ cluster and binuclear center in the mixed valence state $Fe^{I}Fe^{II}$. One-electron reduction can take place either on the cubane subsite leading to $[4Fe\text{-}4S]^{+}Fe^{I}Fe^{II}$ or on the binuclear subsite yielding $[4Fe\text{-}4S]^{2+}Fe^{I}Fe^{I}$ analogous to the "native" H_{red}-state. Both configurations are expected to be EPR silent due to the strong exchange couplings in the H-cluster. Spin counting (see Supporting Information) confirmed that the reduced CrHydA1(pdt) hybrid is indeed EPR silent.

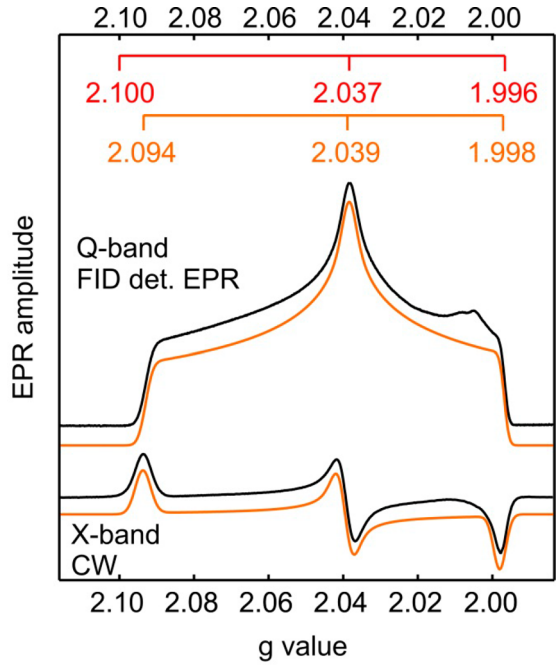

Figure 8. X-band continuous wave and Q-band FID detected EPR spectra (black) and simulations (orange) obtained for the oxidized form of CrHydA1(pdt) measured at 20 K. For comparison the corresponding g values of the H_{ox} state of the native enzyme are presented in red at the top of the figure.[26]

The shift of the FTIR band positions between reduced and oxidized forms is very small; for the CO ligands it lies in the range between 3 and 12 cm^{-1}. The same small shift is observed for the two CO inhibited states in the native system (*vide supra*). Following the same arguments this would suggest that the reduction occurs on the $[4Fe\text{-}4S]_H$ subcluster.

In principle it can be rationalized that the lack of a protonatable headgroup on the binuclear subsite in CrHydA1(pdt) would lead to a decrease of its redox potential since proton coupled electron transfer (PCET) would be inhibited.[45] This would then favor a reduction of the cubane part of the H-cluster. This argument, however, does not explain why the resulting redox potential of the cubane subcluster is even higher (−345 mV) than that of the H_{ox}-H_{red} transition in the native system (−400 mV). A similar argument can be invoked for the redox behavior of CrHydA1(adt) in the H_{ox}-CO state. The extrinsic donor ligand (CO) will

dx.doi.org/10.1021/ja503390c | J. Am. Chem. Soc. 2014, 136, 11339−11346

shift the electron density in the binuclear subsite toward the proximal iron: While the binuclear subsite in H_{ox} is valence delocalized, H_{ox}-CO shows a $Fe(I)_pFe(II)_d$ configuration.[27,46] A similar trend is observed in model systems but there the transition is from $Fe(II)_pFe(I)_d$ in H_{ox} models to $Fe(1.5)_pFe(1.5)_d$ in H_{ox}-CO models.[47,48] These complexes are shown to become oxidized easier.[49] In analogy, a similar effect could be expected for the H-cluster. Indeed, in this case the resulting midpoint potential (−470 mV) is lower than that of the regular CrHydA1(adt) $H_{ox} \rightarrow H_{red}$ transition (−400 mV).

4. CONCLUSIONS

We identified two new redox states in [FeFe] hydrogenases in which the $[4Fe\text{-}4S]_H$ subsite is reduced while the binuclear part remains mixed valence (Fe^IFe^{II}). For both species: $H^{adt}{}_{red'}$-CO and $H^{pdt}{}_{red}$ it can be argued that the redox potential of the binuclear part is lowered by changes of the catalytic site of the H-cluster, i.e., modification of the aza-dithiol bridge to propanedithiol or blocking the open coordination site in the native H-cluster by CO. This leads to a redirection of the electron flow from the binuclear part toward the $[4Fe\text{-}4S]_H$ subsite. Therefore, it can be concluded that the electronic structure of the H-cluster is governed by a strong redox coupling between the two subsites which also must be relevant for its catalytic properties.

We also demonstrated that extrinsic CO binds both in the H_{ox} and $H_{red'}$ state of the native H-cluster. The binding of CO to $H_{red'}$, however, causes a change of the redox equilibrium between the two subsites and induces a transfer of the redox equivalent from the Fe^IFe^I binuclear subcluster to the $[4Fe\text{-}4S]_H$ unit leaving the binuclear part in the Fe^IFe^{II} state. It can therefore be concluded that CO exclusively binds to the divalent distal iron.

Intriguingly, the (effective) redox potential of the $[4Fe\text{-}4S]_H$ subcluster amounts to −470 mV for both the H_{ox}-CO to $H_{red'}$-CO transition and the H_{red} to H_{sred} transition. Apparently, the redox properties of the $[4Fe\text{-}4S]_H$ subcluster do not change when the binuclear subcluster is in the $Fe^IFe^{II}CO_{ext}$ or Fe^IFe^I configuration.

Although the CrHydA1(pdt) is oxygen sensitive like CrHydA1(adt), CO does not seem to bind to CrHydA1(pdt). In native CrHydA1 the adt bridge is conformationally controlled by weak hydrogen bridges to the surrounding amino acid site chains. These interactions are absent in CrHydA1(pdt).We must therefore conclude that the conformation of the dithiol bridge plays an important role in controlling access to the exchangeable site at the distal iron.

■ ASSOCIATED CONTENT

Supporting Information

FTIR electrochemical data processing, determination of the redox midpoint potentials, ^{13}CO exchange experiments, spin counting, and associated figures. This material is available free of charge via the Internet at http://pubs.acs.org.

■ AUTHOR INFORMATION

Corresponding Authors

edward.reijerse@cec.mpg.de
wolfgang.lubitz@cec.mpg.de

Notes

The authors declare no competing financial interest.

■ ACKNOWLEDGMENTS

This work builds on our collaborative project with Marc Fontecave and Vincent Artero (Paris/Grenoble) who laid the foundation for the technique of artificial maturation. We gratefully acknowledge their contribution. We would like to thank Gudrun Klihm for her excellent technical support in the EPR experiments. Furthermore, the Max Planck Society is gratefully acknowledged for its generous financial support. Also support from DFG (HA255/2-1) and Volkswagen Foundation (Project ref. 90352) is gratefully acknowledged.

■ REFERENCES

(1) Miyake, J.; Igarashi, Y.; Rögner, M. *Biohydrogen III*; Elsevier: Amsterdam, 2004.
(2) Rand, D. A. J.; Dell, R. M. *Hydrogen Energy Challenges and Prospects*; RSC Publishing: Cambridge, 2008.
(3) Mertens, R.; Liese, A. *Curr. Opin. Biotechnol.* **2004**, *15*, 343.
(4) Kim, J. Y. H.; Cha, H. J. *Korean J. Chem. Eng.* **2013**, *30*, 1.
(5) Jugder, B.-E.; Welch, J.; Aguey-Zinsou, K.-F.; Marquis, C. P. *RSC Adv.* **2013**, *3*, 8142.
(6) Bockris, J. O. M. *Int. J. Hydrogen Energy* **2013**, *38*, 2579.
(7) Lubitz, W.; Ogata, H.; Rüdiger, O.; Reijerse, E. *Chem. Rev.* **2014**, *114*, 4081.
(8) Vignais, P. M.; Billoud, B. *Chem. Rev.* **2007**, *107*, 4206.
(9) *Hydrogen as a Fuel: Learning from Nature*, Cammack, R. F. M.; Robson, R., Eds.; Taylor & Francis: London, 2001.
(10) *Chemical Energy Storage*; Schlögl, R., Ed.; De Gruyter: Berlin, 2013.
(11) *Molecular Solar Fuels*; Wydrzynski, T. J., Hillier, W., Eds. Royal Society of Chemistry: Cambridge, 2012.
(12) Stripp, S. T.; Happe, T. *Dalton Trans.* **2009**, 9960.
(13) Hatchikian, E. C.; Forget, N.; Fernández, V. M.; Williams, R.; Cammack, R. *Eur. J. Biochem.* **1992**, *209*, 357.
(14) Nicolet, Y.; de Lacey, A. L.; Vernède, X.; Fernández, V. M.; Hatchikian, E. C.; Fontecilla-Camps, J. C. *J. Am. Chem. Soc.* **2001**, *123*, 1596.
(15) Lemon, B. J.; Peters, J. W. *Biochemistry* **1999**, *38*, 12969.
(16) Peters, J. W.; Lanzilotta, W. N.; Lemon, B. J.; Seefeldt, L. C. *Science* **1998**, *282*, 1853.
(17) Nicolet, Y.; Piras, C.; Legrand, P.; Hatchikian, C. E.; Fontecilla-Camps, J. C. *Structure* **1999**, *7*, 13.
(18) Fontecilla-Camps, J. C.; Volbeda, A.; Cavazza, C.; Nicolet, Y. *Chemi. Rev.* **2007**, *107*, 4273.
(19) Silakov, A.; Wenk, B.; Reijerse, E.; Lubitz, W. *Phys. Chem. Chem. Phys.* **2009**, *11*, 6592.
(20) Siegbahn, P. E. M.; Tye, J. W.; Hall, M. B. *Chem. Rev.* **2007**, *107*, 4414.
(21) Nicolet, Y.; Cavazza, C.; Fontecilla-Camps, J. C. *J. Inorg. Biochem.* **2002**, *91*, 1.
(22) Pandey, A. S.; Harris, T. V.; Giles, L. J.; Peters, J. W.; Szilagyi, R. K. *J. Am. Chem. Soc.* **2008**, *130*, 4533.
(23) Schilter, D.; Rauchfuss, T. B. *Angew. Chem., Int. Ed.* **2013**, *52*, 13518.
(24) Berggren, G.; Adamska, A.; Lambertz, C.; Simmons, T.; Esselborn, J.; Atta, M.; Gambarelli, S.; Mouesca, J.; Reijerse, E.; Lubitz, W.; Happe, T.; Artero, V.; Fontecave, M. *Nature* **2013**, *499*, 66.
(25) Esselborn, J.; Lambertz, C.; Adamska-Venkatesh, A.; Simmons, T.; Berggren, G.; Noth, J.; Siebel, J.; Hemschemeier, A.; Artero, V.; Reijerse, E.; Fontecave, M.; Lubitz, W.; Happe, T. *Nat. Chem. Biol.* **2013**, *9*, 607.
(26) Adamska, A.; Silakov, A.; Lambertz, C.; Rüdiger, O.; Happe, T.; Reijerse, E.; Lubitz, W. *Angew. Chem., Int. Ed.* **2012**, *51*, 11458.
(27) Silakov, A.; Reijerse, E. J.; Albracht, S. P. J.; Hatchikian, E. C.; Lubitz, W. *J. Am. Chem. Soc.* **2007**, *129*, 11447.
(28) Silakov, A.; Kamp, C.; Reijerse, E.; Happe, T.; Lubitz, W. *Biochemistry* **2009**, *48*, 7780.
(29) Armstrong, F. A. *Photosynth. Res.* **2009**, *102*, 541.

(30) Pierik, A. J.; Hulstein, M.; Hagen, W. R.; Albracht, S. P. J. *Eur. J. Biochem.* **1998**, *258*, 572.
(31) Albracht, S. P. J.; Roseboom, W.; Hatchikian, E. C. *J. Biol. Inorg. Chem.* **2006**, *11*, 88.
(32) Roseboom, W.; de Lacey, A. L.; Fernández, V. M.; Hatchikian, E. C.; Albracht, S. P. J. *J. Biol. Inor. Chem.* **2006**, *11*, 102.
(33) Baffert, C.; Bertini, L.; Lautier, T.; Greco, C.; Sybirna, K.; Ezanno, P.; Etienne, E.; Soucaille, P.; Bertrand, P.; Bottin, H.; Meynial-Salles, I.; De Gioia, L.; Léger, C. *J. Am. Chem. Soc.* **2011**, *133*, 2096.
(34) Le Cloirec, A.; Best, S. P.; Borg, S.; Davies, S. C.; Evans, D. J.; Hughes, D. L.; Pickett, C. J. *Chem. Commun.* **1999**, 2285.
(35) Li, H. X.; Rauchfuss, T. B. *J. Am. Chem. Soc.* **2002**, *124*, 726.
(36) Schmidt, M.; Contakes, S. M.; Rauchfuss, T. B. *J. Am. Chem. Soc.* **1999**, *121*, 9736.
(37) Kuchenreuther, J. M.; Grady-Smith, C. S.; Bingham, A. S.; George, S. J.; Cramer, S. P.; Swartz, J. R. *PLoS One* **2010**, *5*, e15491.
(38) Moss, D.; Nabedryk, E.; Breton, J.; Mäntele, W. *Eur. J. Biochem.* **1990**, *187*, 565.
(39) Reijerse, E.; Lendzian, F.; Isaacson, R.; Lubitz, W. *J. Magn. Reson.* **2012**, *214*, 237.
(40) Stoll, S.; Schweiger, A. *J. Magn. Reson.* **2006**, *178*, 42.
(41) Goldet, G.; Brandmayr, C.; Stripp, S. T.; Happe, T.; Cavazza, C.; Fontecilla-Camps, J. C.; Armstrong, F. A. *J. Am. Chem. Soc.* **2009**, *131*, 14979.
(42) Fourmond, V.; Greco, C.; Sybirna, K.; Baffert, C.; Wang, P. H.; Ezanno, P.; Montefiori, M.; Bruschi, M.; Meynial-Salles, I.; Soucaille, P.; Blumberger, J.; Bottin, H.; De Gioia, L.; Léger, C. *Nat. Chem.* **2014**, *6*, 336.
(43) Foster, C. E.; Kraemer, T.; Wait, A. F.; Parkin, A.; Jennings, D. P.; Happe, T.; McGrady, J. E.; Armstrong, F. A. *J. Am. Chem. Soc.* **2012**, *134*, 7553.
(44) De Lacey, A. L.; Stadler, C.; Fernández, V. M.; Hatchikian, E. C.; Fan, H. J.; Li, S. H.; Hall, M. B. *J. Biol. Inorg. Chem.* **2002**, *7*, 318.
(45) Camara, J. M.; Rauchfuss, T. B. *Nat. Chem.* **2012**, *4*, 26.
(46) Silakov, A.; Reijerse, E. J.; Lubitz, W. *Eur. J. Inorg. Chem.* **2011**, 1056.
(47) Silakov, A.; Shaw, J. L.; Reijerse, E. J.; Lubitz, W. *J. Am. Chem. Soc.* **2010**, *132*, 17578.
(48) Silakov, A.; Olsen, M. T.; Sproules, S.; Reijerse, E. J.; Rauchfuss, T. B.; Lubitz, W. *Inorg. Chem.* **2012**, *51*, 8617.
(49) Gloaguen, F.; Rauchfuss, T. B. *Chem. Soc. Rev.* **2009**, *38*, 100.